



Titre: Title:	Uplift of the Longmen Shan range and the Wenchuan earthquake
Auteurs: Authors:	Zhiqin Xu, Shaocheng Ji, Haibing Li, Liwei Hou, Xiaofang Fu, & Zhihui Cai
Date:	2008
Туре:	Article de revue / Article
Référence: Citation:	Xu, Z., Ji, S., Li, H., Hou, L., Fu, X., & Cai, Z. (2008). Uplift of the Longmen Shan range and the Wenchuan earthquake. Episodes, 31(3), 291-301. https://doi.org/10.18814/epiiugs/2008/v31i3/002

Document en libre accès dans PolyPublie Open Access document in PolyPublie

URL de PolyPublie: PolyPublie URL:	https://publications.polymtl.ca/5179/
Version:	Version officielle de l'éditeur / Published version Révisé par les pairs / Refereed
Conditions d'utilisation: Terms of Use:	CC BY-NC

Document publié chez l'éditeur officiel Document issued by the official publisher

Titre de la revue: Journal Title:	Episodes (vol. 31, no. 3)
Maison d'édition: Publisher:	International Union of Geological Sciences
URL officiel: Official URL:	https://doi.org/10.18814/epiiugs/2008/v31i3/002
Mention légale: Legal notice:	

by Zhiqin Xu¹, Shaocheng Ji², Haibing Li¹, Liwei Hou³, Xiaofang Fu³, and Zhihui Cai¹

Uplift of the Longmen Shan range and the Wenchuan earthquake

- 1 Key Laboratory of Continental Dynamics, Ministry of Land and Resources; Institute of Geology, Chinese Academy of Geological Sciences; Beijing 100037, China. *E-mail:* xzq@ccsd.cn
- 2 Department of Civil, Geological and Mining Engineering, Ecole Polytechnique de Montreal, Montreal, Quebec, H3C 3A7, Canada.
- 3 Department of Land and Resources of Sichuan Province, Chengdu 610072, China.

The 12 May 2008 Wenchuan earthquake ($M_s=8.0$) struck on the Longmen Shan foreland thrust zone. The event took place within the context of long-term uplift of the Longmen Shan range as a result of the extensive eastward-extrusion of crustal materials from the Tibetan plateau against the rheologically strong crust of the Sichuan Basin. The Longmen Shan range is characterized by a Pre-Sinian crystalline complex constrained by the Maoxian-Wenchuan-Kangding ductile detachment at the western margin and the Yingxiu-Beichuan-Luding ductile thrust at the eastern margin. The Longmen Shan uplift was initiated by intracontinental subduction between the Songpan-Ganzi terrane and the Yangtze block during the Pre-Cenozoic. The uplift rate was increased considerably by the collision between the Indian and Eurasian plates since ~50 Ma. The Wenchuan earthquake resulted in two major NE-striking coseismic ruptures (i.e., the ~275 km long Yingxiu-Beichuan-Qingchuan fault and the ~100 km long Anxian-Guanxian fault). Field investigations combined with focal solutions and seismic reflection profiles suggest that the coseismic ruptures are steeply dipping close-topure reverse or right reverse oblique slip faults in the ~15 km thick upper crust. These faults are unfavorably oriented for frictional slip in the horizontally compressional regime, so that they need a long recurrence interval to accumulate the tectonic stress and fluid pressure to critically high levels for the formation of strong earthquakes at a given locality. It is also found that all the large earthquakes ($M_s > 7.0$) occurred in the fault zones across which the horizontal movement velocities measured by the GPS are markedly low (<3 mm/yr). The faults, which constitute the northeastern fronts of the enlarging Tibetan plateau against the strong Sichuan Basin, Ala Shan and Ordos blocks, are very destructive, although their average recurrence intervals are generally long.

Introduction

On 12 May 2008, a destructive earthquake of magnitude $8.0\,M_s$ according to the China Earthquake Administration and 7.9 M_w according to the US Geological Survey struck the Longmen Shan region of Sichuan Province, China. This earthquake was named the Wenchuan earthquake as its epicenter was located in the administrative region of Wenchuan County (Figure 1). The epicenter (31.021°N, 103.367°E) was ~80 km west-northwest of Chengdu, the capital of Sichuan. The earthquake was felt as far away as Beijing (1,500 km away) and Shanghai (1,700 km away) and also in nearby countries. Within the first 112 days after the mainshock, there were some 27,000 aftershocks in total, with the strongest M_s=6.4 on 25 May 2008. During the same period, 8 M_s≥6 and 39 M_s≥5 aftershocks occurred, all with hypocenters in the 10-20 km depth range. The severity of the mainshock is estimated as high as X to XI on the scale of the Mercalli Intensity rating. The quake resulted in a total disaster area of 440,000 km², of which an area of 125,000 km² was seriously affected: most buildings collapsed, bridges were destroyed, railroad tracks were badly bent, and large numbers of landslides occurred, affecting a total of 46.24 million people in Sichuan, Shaanxi and Gansu Provinces. A government report published on 4 September 2008 stated that 69,226 people were confirmed dead, 374,643 injured and 17,939 missing. More than 7.7891 million homes collapsed and 24.59 million were damaged. The earthquake induced strong ground movements that caused a tremendous amount of hazards including avalanches, landslides, mudflows, soil liquefaction, and large barrier lakes.

The Wenchuan earthquake and aftershocks occurred in the northeast-trending Longmen Shan fault zone, which lies along the eastern margin of the Tibetan plateau as a result of crustal extrusion against the rheologically strong lithosphere of the Sichuan Basin, which is a part of the Yangtze block. The Longmen Shan range is a continental foreland accretional wedge thrust on the Mesozoic-Cenozoic oil-bearing Sichuan Basin (Figure 1). A series of thrust faults (e.g., the Wenchun-Maoxian, Yingxiu-Beichuan and Anxian-Guanxian faults) have been recognized. The epicenter of the 12 May 2008 mainshock (31.01°N, 103.38°E) was located in the western outskirts of Yingxiu village, through which the Yingxiu-Beichuan fault broke.

The Wenchuan-Maoxian fault is also called the western margin fault of the Longmen Shan. This fault has been considered a normal ductile shear zone (Fig. 1, Xu et al, 1992), a thrust (Chen et al., 1995) and a Triassic transpressional fault (Wang et al., 2001). Considering extremely steep gradients in both crustal thickness (from ~40 km in the east to 60–65 km in the west) and topographic elevation (from 500 m above sea level in the Sichuan Basin to 4,000–6,000 m on the plateau) across the 40–50 km wide Longmen Shan range, several tectonic models have been proposed for the range in terms of its uplift mechanism: (1) The Longmen Shan uplift resulted from a combination of foreland thrusting and backland normal faulting in response to eastward extrusion and enlargement of the high Tibetan plateau (Xu et al., 1999; Xu et al., 2007). (2) The surface uplift of the

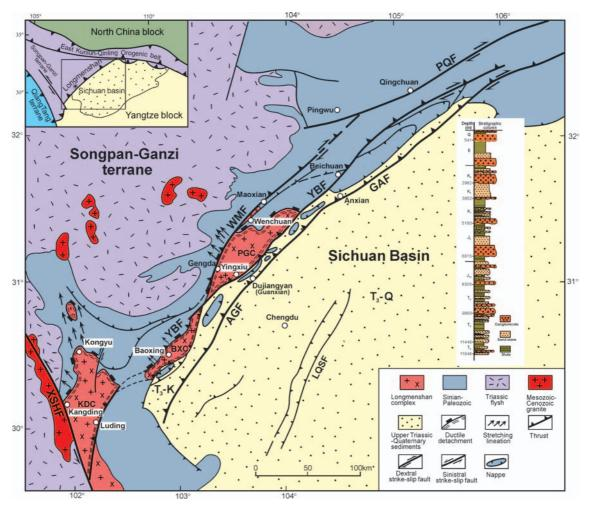


Figure 1 A simplified geological map of the Longmen Shan range and its adjacent areas.

WMF: Wenchuan-Maoxian fault; YBF: Yingxiu-Beichuan fault; GAF: Guanxian-Anxian fault; PQF: Pingwu-Qingchuan fault; XSHF: Xianshuihe fault; LQSF: Longquan Shan fault. Inset: Regional-scale setting of the Longmen Shan range between the Songpan-Ganzi terrane and the Yangtze block.

Longmen Shan is related to eastward channel flow of low-viscosity (probably partially molten) materials in the mid- to lower crust of the eastern Tibetan plateau since about 4 Ma (Royden et al., 1997; Clark and Royden, 2000). (3) Based on the fact that the thrusting-induced uplift started in late Tertiary and early Cretaceous, and has continued to the present-day since the mid-Cretaceous, Wallis et al. (2003) suggested that the crustal shortening of the Longmen Shan was not related to the eastward extrusion of the Tibetan plateau that took place after the collision between the India and Asia plates at ~45 Ma.

Global positioning system (GPS) data showed that, different from the eastern Tibetan plateau with northeastward displacement rates of 15–20 mm/yr (Figure 2), the convergence across the Longmen Shan is slow (<3 mm/yr). GPS data were indeed misinterpreted as an evidence for inactivity of the Longmen Shan fault zone and thus impossibility of strong earthquakes in the region (Chen et al., 2000; Zhang et al., 2004).

In this paper, we discuss the relationship between the uplift process of the Longmen Shan range and the origin of the Wenchuan earthquake, based on new geological and geophysical observations.

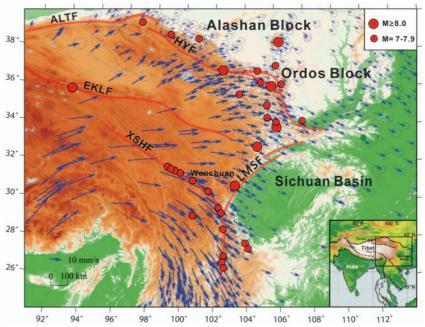


Figure 2 GPS velocities in and around the eastern Tibetan plateau with respect to stable Eurasia. (After Zhang et al., 2004)

Red dots: earthquakes ($M \ge 7.0$). Inset: Regional-scale setting of Tibetan Plateau. ALTF: Altyn Tagh fault; EKLF: East Kunlun fault; LMSF: Longmen Shan Fault; XSHF: Xianshuihe fault.

Tectonic setting of the Longmen Shan

The Longmen Shan range lies between the Songpan-Ganzi terrane (a Triassic orogenic belt) and the Sichuan Mesozoic-Cenozoic foreland basin on the Yangtze block. The mountains are mainly composed of Precambrian metamorphic rocks (700–800 Ma), with small amounts of Neoproterozoic volcanic rocks and Sinian to early-middle Triassic marine sedimentary rocks. A series of thrust faults and nappes occur along the eastern margin of the Longmen Shan, and the entire complex was overlapped eastward on the Sichuan foreland basin (Figure 1). Four tectonic units can be distinguished.

The complex belt of the Longmen Shan crystalline basement

The NNE-SSW-tending Longmen Shan basement complex belt consists from north to south of the Pengguan complex, the Baoxing complex and the Kangding complex. These complexes consist of diorite, quartz diorite, granodiorite, plagioclase granite, biotite granite, K-rich granite and intruded mafic veins with ages of 757–805 Ma. The mafic intrusion is inferred to indicate that the Yangtze crystalline basement was a rifted fragment of Rodinia. The Neo-Protero-

zoic volcanic rocks and graphite marble, the Sinian-Silurian conglomerate, siltite, slate and silicalite, the Carboniferous to low-to-mid Triassic limestone as well as the upper Triassic coal strata, all overlap on the older complex.

The Longmen Shan foreland thrusting wedge

Seismic lines across the Longmen Shan (Song et al., 1989; Jia et al., 2003) (Figure 3) reveal that the eastern edge of the range is a foreland accretionary wedge composed of imbricated thrust sheets bounded by a series of thrust faults mainly including the Maoxian-Wenchuan thrust fault, the Yingxiu-Beichuan thrust fault and the Anxian-Guanxian thrust fault, all having eastward displacement vectors. The crystalline complex, Neoproterozoic volcanic rocks and Sinian-Middle Triassic marine sediments are involved in the thrust sheets. As indicated by the seismic profiles across the range, the thrust planes have a listric geometry, dipping steeply to the west in the uppermost crust and then gradually dipping westward in the middle crust. Many small nappes, which are composed of the Devonian-Middle Triassic limestone overridden on the upper Triassic coal strata of the Sichuan foreland basin, lie at the front of the Longmen Shan complex (Figure 3).

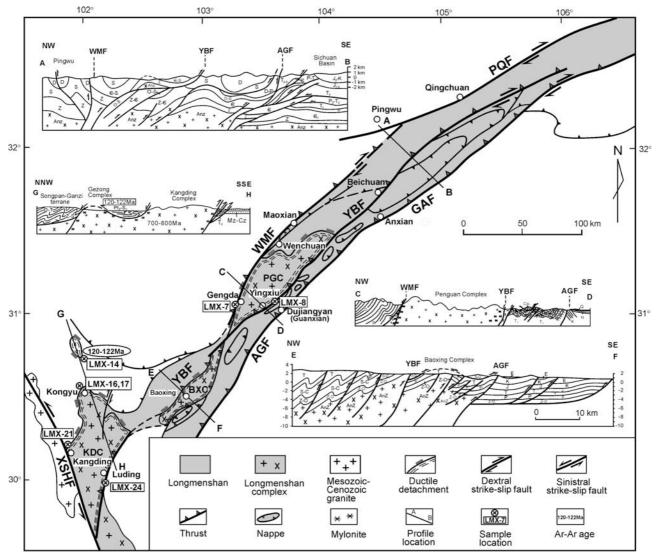


Figure 3 Tectonic map and cross sections of the Longmen Shan and adjacent areas.

WMF: Wenchuan-Maoxian fault; YBF: Yingxiu-Beichuan fault; GAF: Guanxian-Anxian fault; PQF: Pingwu-Qingchuan fault, XSHF: Xianshuihe fault, LQSF: Longquan Shan fault. Locations of samples for quartz fabric analyses are also indicated.

The Sichuan foreland basin

The Sichuan Basin is a composite basin that has a Paleozoic to Cenozoic complete strata sequence with a bulk thickness of 6,000-12,000 m. The Upper Triassic-Quaternary strata are continental deposits with thicknesses of 1,500-3,000 m, 2,000-5,000 m, ~2,000 m and ~1,100 m for the upper Triassic, Jurassic, Cretaceous, and Cenozoic, respectively. The clastic rocks of the Sichuan Basin include conglomerate and coal strata with a bulk thickness of several thousand meters, having accumulated during the end of the Late Triassic. Considering the Lower-Middle Jurassic strata overlapping unconformably upon the foreland border of the thrust, we suggest that the molasses formed from the end of the late Triassic to Jurassic as a result of the foreland basin of the Songpan-Ganzi orogenic belt. The strata of the late Mesozoic-Eocene series have an accumulated thickness of 3,400 m, with several groups of molasses developed. These molasses are equally characteristic of the foreland basin. Since the Cenozoic folds and thrust structures have developed in the foreland basin due to the NW-SE-oriented compression. They are linked to the lateral extrusion of crustal materials from the eastern Tibetan plateau. The basement of the Sichuan foreland basin is composed mainly of granite and dellenite, the Rb-Sr whole-rock isochron ages of which are 741 Ma and 702 Ma, respectively. These ages are comparable to those of the Longmen

Shan crystalline complex.

The Songpan-Ganzi terrane

The Songpan-Ganzi terrane is a Triassic orogenic belt, displaying a triangle shape, 1,000 km wide in the NS direction and 2,000 km long in the EW direction. This terrane is bounded by the East Kunlun terrane in the north, the Qiangtang terrane in the southwest, and the Longmen Shan range in the east. The formation of this orogenic belt was related to the closures of the Kunlun-Animaqin oceanic basin in the north and the Jinshajiang Paleotethys oceanic basin in the southwest, and to the collision among the eastern Kunlun terrane, the Songpan-Ganzi terrain and the Qiangtang terrane during the upper Triassic. The Songpan-Ganzi orogenic belt was offset 80-90 km by the NW-SE-trending, Xianshuihe left-lateral strike-slip fault during the last 20 Ma: the NE part being the Danba tectonic unit and the SW part being the Muli tectonic unit (Xu et al., 1996). Both units have a metamorphic basement similar to the Longmen Shan crystalline complex in terms of both lithology and formation age.

Pre-Cenozoic Longmen Shan extrusion structure

A ductile thrust zone dipping steeply to the west lies between the Longmen Shan crystalline complex and the Neo-Protorozoic metavolcanic rocks above and on the eastern margin of the Longmen Shan. Brittle deformation overprinted on the early ductile thrusting formed the so-called Yingxiu-Beichuan thrust fault in the present-day crust above the ductile-brittle transition zone. At the NW margin of the complex, a ductile detachment (i.e., extensional shear zone) dipping steeply to the west between the complex and its covers is characterized by mylonitization and intense plastic shear strain with top-to-west shear sense indicators. This ductile detachment was reactivated

as the brittle Wenchuan-Maoxian thrust fault during the Cenozoic. Obviously, the Longmen Shan complex acted initially as an extrusion structure during the Cretaceous compression, because the ductile detachment (upper boundary) occurred at the western margin whereas the ductile thrust occurred at the eastern margin (lower boundary).

Ductile detachment at the northwestern margin of the Longmen Shan

The ductile detachment at the northwestern margin of the Longmen Shan extends from the western Pengguan complex, through the western Baoxing complex, and finally to the Kangding complex. Generally the detachment dips steeply to the west. In the northwestern Pengguan complex and the northern Kangding complex, however, it dips gently to the north or the northwest.

In the Wenchuan-Gengda area at the western margin of the Pengguan-Baoxing granodioritic complex, the intensely deformed and thinned Neoproterozoic metavolcanic rocks and the Ordovician–Silurian epizonal metamorphic strata overlap on the complex. The ductile detachment between the complex and its covers is characterized by foliation dipping steeply to the west, dip-slip stretching lineation and mylonitization (Figure 4). On the plane parallel to the lin-

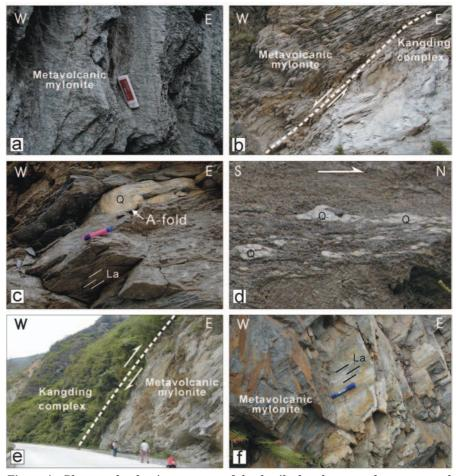


Figure 4 Photographs showing outcrops of the ductile detachment at the western and northern margins of the Longmen Shan complex.

- (a) Metavolcanic mylonite with foliation steeply dipping to the west at Gengda (western margin of the Pengguan complex).
- (b) The detachment developed in metavolcanic and granitic mylonites at the western margin of the Kangding complex.
- (c-d) A gentle detachment developed in the Silurian phillite at the northern margin of the Kangding complex where A-fold (c), rotational quartz porphyroclasts and quartzite lenses (d) indicate a top-to-northwest normal shear.
- (e) Ductile thrust between the overlying Kangding complex and underlying upper Proterozoic volcanic rocks.
- (f) Inverse stretching lineations on the foliation plan steeply dipping to the west, developed in a metavolcanic mylonite in the ductile thrust at the eastern margin of the Kangding complex.

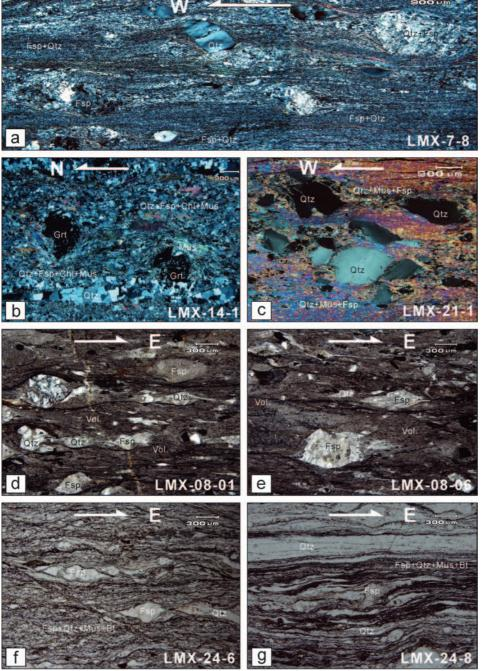


Figure 5 Microphotographs showing shear deformation in the ductile detachment along the western and northern margins of the Longmen Shan complex.

- (a) Rotational quartz porphyroclasts (Qtz) and felsic aggregates (Fsp+Qtz) (sample LMX-7-8) showing a top-to-west shear from a metavolcanic mylonite (matrix is composed of quartz, feldspar, chlorite and muscovite) at Gengda (the western margin of the Pengguan complex).
- (b) Pressure shadow of Garnet porphyroclasts from phyllonite (matrix is composed of mylonitic quartz, feldspar, chlorite and muscovite) (sample LMX-14-1) showing a top-to-east shear along the northern margin of the Kangding complex.
- (c) Rotational quartz porphyroclasts from granitic mylonite (matrix is composed of quartz, feldspar and muscovite) (sample LMX-21-1) showing a top-to-east shear along the western margin of the Kangding complex.
- (d-e) Quartz and feldspar porphyroclasts in the metavolcanic mylonites (samples LMX-08-01 and LMX-08-06) from the Bajiaomiao of Dujianyan show a top-to-east ductile thrust shear for the eastern margin of the Pengguan complex.
- (f-g) Rotational quartz and feldspar porphyroclasts in granitic mylonites (matrix is composed of feldspar, quartz, muscovite and biotite) (samples LMX-24-6 and LMX-24-8) from Luding indicate a top-to-east ductile thrust shear for the eastern margin of the Kangding complex.

eation and perpendicular to the foliation (i.e., the XZ plane), σ - and δ -shaped asymmetric feldspar or quartz porphyroclasts indicate consistently a top-to-west shear sense (Figure 5). Lattice-preferred orientations (LPOs) of quartz from five typical granitic mylonites and phyllonites (samples LMX7-2, LMX 3, LMX 8, LMX 11 and LMX 13), measured using the electron backscatter diffraction (EBSD) techniques (Figure 6a), indicate that quartz deformed by dislocation glide using slip system varying from $\{10\bar{1}0\}$ <a>><a>, through $\{10\bar{1}1\}$ <a>><a>, and finally to $\{0001\}$ <a>><a>. The fabric evolution suggests that the deformation temperature varied from early moderate temperature (~550°C) to late low temperature (~350°C). The LPO asymmetry with respect to the structural framework (X-Y-Z) displays a top-to-the-northwest shear sense.

The northern portion of the Kangding complex exposed in the Kongyu-Mingai area is overridden by intensively sheared Neo-Proterozoic metavolcanic rocks with or without thinned Z-S epizonal metamorphic strata. The ductile detachment is composed of granitic mylonite and phyllite with foliation dipping gently towards NNW,

nearly NS-aligned stretching lineation, A-type folds and sheath folds. Rotated limestone blocks (boudins) and σ -shaped quartz porphyroclasts in the Silurian phyllite indicate the top-to-north shear (Figures 4, 5).

The Gezong complex, which lies 18 km to the north of Kongyu, is composed of granodiorite (U-Pb zircon age is 771 Ma, similar to that of the Kangding complex). The thinned and deformed Neoproterozoic metavolcanic rocks and the Sinian-Silurian epizonal metamorphic rocks (e.g., conglomerate and gravel phyllite) covered the complex with an interface of mylonitization. This ductile detachment joins southward with that at the northern margin of the Kangding complex (Figures 1, 2). Quartz LPOs from 5 phyllonite samples, among which three (LMX17-1, LMX17-2 and LMX17-4) were collected from the Kongyu area (i.e., the northern Kangding complex) and two (LMX14-1 and LMX14-2) from the southern Gezong complex, were measured using the EBSD techniques. The fabric results (Figure 6b) reveal that the prevailing dislocation slip system varied from {1010}<a>><a>, then {1011}<a>><a>, finally to {0001}<a><<a><a> (~550°C–350°C) for the northern Kangding complex, and

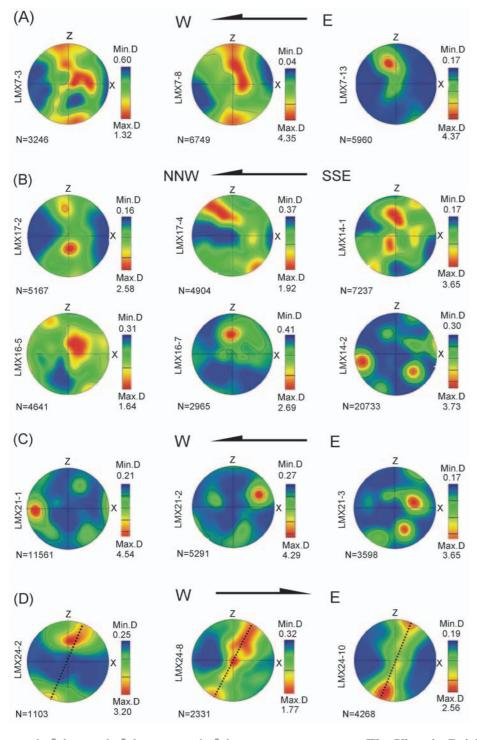


Figure 6 LPO's of quartz from the mylonites of the ductile detachment and ductile thrust, measured using the EBSD techniques.

- (a) Samples LMX7-3, LMX7-8 and LMX7-13 collected from Gengda at the western margin of the Pengguan complex.
- (b) Samples LMX-17-2 and LMX17-4 from Kongyu at the northern edge of the Kangding complex, and samples LXM16-5 (phyllitic conglomerate), LXM16-7 (granitic mylonite) and LMX14-1 and LMX14-2 (garnet-bearing quartz schist) from Gezong at the northern margin of the Kangding complex.
- (c) Samples LMX21-1, LMX21-2, and LMX 21-3 from Paoma Shan at the western margin of the Kangding complex.
- (d) Samples LMX24-2, LMX24-8, and LMX-24-10) from Ludingqiao at the eastern edge of the Kangding complex. X and Z are parallel to lineation and normal to foliation, respectively. N: number of measurement points. Min. D and Max. D represent the minimum and maximum densities, respectively.

from $\{10\bar{1}0\}$ <c> to $\{10\bar{1}0\}$ <a> then to $\{10\bar{1}1\}$ <a> (~650°C–450°C) for the southern Gezong complex. The quartz fabric asymmetry yields consistently the same shear sense: top to the northwest.

The ductile detachment between the Kangding complex and the metavolcanic rocks dips more steeply westward. σ-shaped feldspar or quartz porphyroclasts in the granitic mylonite near the Kangding bus station indicate a top-to-west shear sense (Figures 4, 5). Three mylonites (samples LMX-21-1, LMX-21-2, LMX-21-3) from the Paoma Shan at the western margin of the Kangding complex were collected for the EBSD measurement of quartz LPOs (Figure 6c). Dislocation slip systems are inferred to display a transition from {1010}<c> to {1011}<a>. The fabric evolution indicates a change in deformation temperature from ~650°C to ~450°C. The LPO asymmetry yields a top-to-west shear.

The Yingxiu-Beichuan ductile thrust at the eastern margin of the Longmen Shan complex

The Beichuan-Yingxiu ductile thrust, which lies between the eastern margin of the Longmen Shan complex and the Neo-Proterozoic metavolcanic rocks, is marked by a 200–300 m thick belt of granitic and metavolcanic mylonites. The mylonitic foliation dips deeply to the west. S-C structures and porphyroclast systems on the XZ plane indicate a top-to-east shear. LPOs of quartz from 5 mylonite samples (LMX24-2, LMX24-3, LMX24-5, LMX24-8, LMX24-10) collected from Ludingqiao, eastern margin of the Kangding complex (Figure 6d), suggest a slip system transition from $\{10\bar{1}0\}$ <a> \rightarrow $\{0001\}$ <a> $(\sim550^{\circ}\text{C}-350^{\circ}\text{C})$ and a top-to-east shear sense

⁴⁰Ar/³⁹Ar ages of the Longmen Shan ductile detachment

Two samples (LMX-14-2, LMX-14-3) were collected from the metavolcanic mylonites of the ductile detachment at the southern margin of the Gezong complex for biotite $^{40}\mathrm{Ar}/^{39}\mathrm{Ar}$ dating (Table 1 and Figure 7). The total age of 12 temperature stages is 119.4 Ma. Nine moderate and high temperatures stages between 900°C and 1,400°C display a flat plateau age (Tp) of 121.5±1.0 Ma, which corresponds to the cumulative $^{39}\mathrm{Ar}$ percent of 93.8% (Figure 7). The $^{39}\mathrm{Ar}/^{40}\mathrm{Ar}$ – $^{36}\mathrm{Ar}/^{40}\mathrm{Ar}$ inverse-isochron age (Ti) is 122.9±1.4 Ma, having the same uncertainty as the plateau age. The initial $^{40}\mathrm{Ar}/^{36}\mathrm{Ar}$ age is 254±22 Ma (MSWD= 0.64) (Figure 7). The Ar-Ar plateau age of 121.5 Ma represents the age of biotite cooling down to the close temperature (~350°C) of the isotope.

The total age of 12 temperature stages is 122.8 Ma for the sample LMX-14-3 (Figure 7). Several low temperature stages between 500°C and 700°C result in much higher apparent ages, which may have been caused by the influence of nuclear recoil or the alteration of the mineral particle surfaces and have no geological significance. Six high temperature stages between 1,000°C and 1,400°C display a very flat plateau with an age (T_p) of 120.7±1.1 Ma, which corresponds to the cumulative ³⁹Ar percent of 81% (Figure 7). Accordingly, the ³⁹Ar/⁴⁰Ar=³⁶Ar/⁴⁰Ar inverse-isochron age (T_i) is 121.1±1.3 Ma, possessing the same uncertainties as the plateau age. The initial ⁴⁰Ar /³⁶Ar is 287.0±9.2 Ma (MSWD=0.56) (Figure 7),

which has the same error range as the Ar ratio of modern atmosphere. The plateau age of 120.7 Ma represents the value when the biotite cooled down to the close temperature (~350°) of the isotope.

The Ar-Ar plateau ages of biotite from samples LMX-14-2 and LMX-14-3 are consistent within the measurement uncertainty, and

Table 1 Results of 40 Ar/ 39 Ar dating for the biotite from mylonite sample.

T °C	(⁴⁰ Ar/ ³⁹ Ar) _m (³⁶ Ar/ ³⁹ Ar) _m	(³⁷ Ar/ ³⁹ Ar) _m	(³⁸ Ar/ ³⁹ Ar) _m	F	³⁹ Ar (Cum.) %	Age Ma	±1s Ma
LMX-	14-2 biotite	W=50.00	mg J=0.	011825				
500	26.0287	0.0619	0.5541	0.0694	7.7806	0.36	158.8	6.9
600	18.0281	0.0293	0.1919	0.0468	9.3871	1.08	189.9	4.7
700	18.4672	0.0446	0.1234	0.0446	5.2933	1.45	109.5	4.4
800	9.7128	0.0210	0.1125	0.0300	3.5056	6.15	73.3	2.1
900	6.4357	0.0023	0.0104	0.0147	5.7501	29.71	119.1	1.6
1000	6.3456	0.0016	0.0326	0.0179	5.8645	44.32	121.0	1.3
1100	6.1795	0.0013	0.0762	0.0187	5.7994	66.02	121.7	1.3
1150	6.6564	0.0027	0.0373	0.0159	5.8466	67.56	120.6	1.6
1200	6.1873	0.0010	0.0190	0.0139	5.9004	73.13	121.7	1.3
1250	6.1698	0.0007	0.0140	0.0138	5.9569	84.15	122.8	1.5
1300	6.2346	0.0008	0.0274	0.0135	5.9908	95.04	122.8	1.3
1400	6.4464	0.0018	0.0926	0.0139	5.9112	100.00	121.9	1.6
Total	age =119.4 M	a; T _p =121.	5±1.0 Ma;	T _i =122.9±1.4	Ma (MSV	VD=0.64)		
LMX-	14-3 biotite	W=49.6 m	g J=0.011	825				
500	30.9946	0.0698	1.1860	0.0792	10.4592	0.21	210.0	10.0
600	22.8808	0.0103	0.3562	0.0353	19.8697	0.72	380.7	5.0
700	15.2172	0.0133	0.2257	0.0255	11.2908	1.65	226.1	3.8
800	10.4046	0.0137	0.1809	0.0302	6.3506	4.35	130.6	2.6
900	6.4885	0.0030	0.0070	0.0147	5.5960	19.04	115.6	1.3
1000	6.1976	0.0013	0.0074	0.0147	5.8166	33.08	120.0	1.4
1100	6.0981	0.0007	0.0093	0.0139	5.8839	44.76	121.3	1.5
1150	6.1244	0.0008	0.0141	0.0140	5.8829	53.57	121.3	1.3
1200	6.0612	0.0006	0.0097	0.0131	5.8691	68.20	121.0	1.3
1300	6.0427	0.0006	0.0149	0.0136	5.8645	96.86	121.0	1.3
1400	9.3278	0.0124	1.3606	0.0170	5.7762	100.00	119.2	1.7
Total	age =122.8 M	a; $T_p = 120$.	7±1.1 Ma;	T _i =121.1±1.3	Ma (MSV	VD=0.56)		

correspond to the ages of the mylonites (120-122 Ma) when cooling down to $\sim 350^{\circ}$ C. These ages represent the time of the formation of the ductile detachment at the western margin of the Longmen Shan complex.

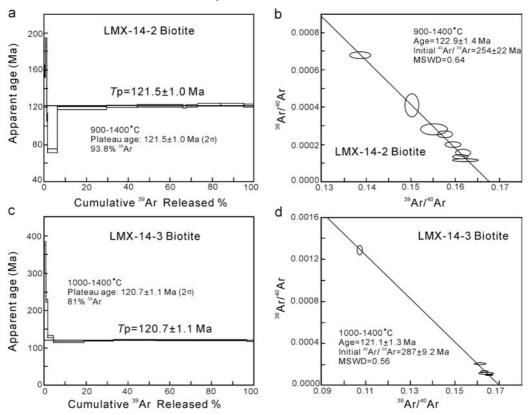


Figure 7 40 Ar/ 39 Ar age spectra and isochron of the biotite from mylonite samples of the Gezong complex.

Coseismic ruptures of the Wenchuan earthquake

Seismic waveform analyses (Table 2) show that the 12 May 2008 $M_s{=}8.0$ mainshock started from a hypocenter on a northwest-dipping fault (azimuth 238°, dip 59°) and propagated unilaterally to the northeast over a distance of ~275 km along the Longmen Shan range from Dujiangyan to Guangyuan (Figure 8). Three principal stresses are determined: σ_1 (302, 06), σ_2 (036, 31), and σ_3 (202, 57). The earthquake, whose tremors lasted for about 2 minutes, was composed of two sub-events of 6–9 m slip (Parsons et al., 2008): the epicentral sub-event underwent oblique right-lateral thrust slip, whereas the northeast sub-event slipped largely right-laterally.

Our field observations of fault outcrops (Figure 9) showed that a main coseismic rupture developed along the Yingxiu-Beichuan-Qingchuan fault over a length of ~275 km and a depth of 15–20 km, and a secondary rupture over a length of ~100 km formed along the southern segment of the Anxian-Guanxian fault (Figure 8). The latter

is referred as the front fault of the Longmen Shan range. Furthermore, two minor surface breaks occur between the two principal ruptures mentioned above: one is ~20 km long, and the other is about 6 km long. These minor faults are equally characterized by SW-to-NE thrusting together with right-lateral slip. From west to east, the NE-trending ruptures dip from nearly vertical to 50°-60° to the northwest (Table 3), and the amounts of net slip (i.e., displacement) also decreases gradually. We observed that the relative displacement of each coseismic surface rupture between the hanging wall and footwall blocks varies considerably with the strike (Figure 9). The maximal vertical and horizontal components of the slip vector which is parallel to the slickensides (Figure 9) are 8.0 m and 10.0 m, respectively. A NE-striking sand liquefaction zone was observed along the surface trace of the Anxian-Guanxian fault from Juyuan town of Dujiangyan to Jiangyou city, indicating the coseismic activation of the deep blind fault that was imaged by previous seismic profiles. Analyses of the INSAR images also reveal certain reactivation of the Wenchuan-Maoxian fault, although no clear coseismic ruptures have been found on the surface between Wenchuan and Maoxian. Several large aftershocks were related to the reactivation of the Wenchuan-Maoxian fault (Figure 8).

Table 2 Focal mechanisms of the mainshock and some aftershocks of the Wenchuan earthquake sequence.

Date	Time	Latitude	Longitude I	Magnitude	Depth	Fault	$\sigma_{\scriptscriptstyle 1}$	σ_{2}	σ_3	Reference
2008-05-12	06:28:04.0	31.00	103.40	8.0	16.0	238, 59	302, 06	036, 31	202, 57	USGS, 2008
2008-05-13	07:07:07.2	30.95	103.20	6.1	10.0	238, 62	301, 08	036, 33	198, 55	USGS, 2008
2008-05-16	05:25:46.3	31.35	103.18	5.9	24.5	233, 71	096, 18	303, 69	189, 09	Global CMT, 2008
2008-05-14	02:54:35.5	31.32	103.38	5.6	12.0	212, 78	077, 07	312, 78	168, 10	Global CMT, 2008
2008-05-12	20:08:48.5	31.42	103.82	5.6	28.4	228, 41	108, 11	013, 27	218, 60	Global CMT, 2008
2008-08-01	08:32:44.6	32.10	104.70	6.1	20.2	210, 67	289, 21	024, 13	145, 65	Global CMT, 2008
2008-05-17	17:08:24.8	32.25	104.90	6.0	14.0	232, 44	136, 01	046, 06	235, 84	Global CMT, 2008
2008-05-25	08:21:49.3	32.55	105.33	6.4	15.0	058, 82	104, 01	197, 78	014, 12	Global CMT, 2008
2008-07-23	19:54:00.0	32.80	105.55	5.6	12.0	012, 45	260, 04	169, 21	002, 68	Global CMT, 2008
2008-08-05	09:49:18.7	32.78	105.48	6.1	12.0	347, 45	071,00	161, 06	341, 84	Global CMT, 2008
2008-05-27	08:37:51.3	32.77	105.58	5.7	15.0	089, 64	308, 31	141, 58	041, 06	Global CMT, 2008
2008-07-24	07:09:00.0	32.82	105.47	6.0	12.2	110, 72	332, 22	164, 68	064, 04	Global CMT, 2008

USGS: http://www.usgs.gov/

Global CMT: http://www.globalcmt.org/

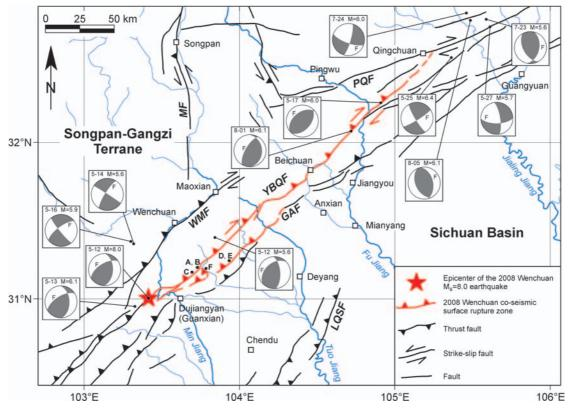


Figure 8 Focal mechanism solutions and coseismic surface ruptures (red lines) of the Wenchuan earthquarke sequence.

YBQF: Yingxiu-Beichuan-Qingchuan fault; GAF: Guanxian-Anxian fault; WMF: Wenchuan-Maoxian fault; LQSF: Longquan Shan fault; PQF: Pingwu-Qingchuan fault; MF: Minjiang fault.



Figure 9 Typical coseismic surface ruptures produced by the Wenchuan earthquake.

- (A–B) A NE-striking, ~ 4.3 m high reverse fault scarp along the Yingxiu-Beichuan rupture zone at Bajiaomiao Village where fault plane dips 72°–80° NW, with remarkable slickensides. Reverse, oblique thrusting.
- (C) A NE-striking, ~2.5 m high flexural scarp of a back-thrust along the Yingxiu-Beichuan rupture zone at Gaoyuan Village.
- (D) A NE-striking, 2.2 m high flexural scarp along the Guanxian-Anxian rupture zone, which went through between two buildings in the Bailu School.
- (E) A NE-striking, 2.2 m high flexural scarp along the Guanxian-Anxian rupture zone cutting the floodplain and bottom of Laojie River.
- (F) A NE-striking flexural scarp joins the Yingxiu-Beichuan and Guanxian-Anxian rupture zones. The horizontal and vertical components of the coseismic slip are 2.7 m and 1.3 m, respectively.

The extensive sequence of the aftershocks is strongly polarized in the NE direction between Yingxiu town and Guangyuan, and extremely asymmetrical with respect to the epicenter of the mainshock. The spatial distribution of the subsequent aftershocks is unambiguously controlled by the faults mentioned above. Stress transfer between the faults (e.g., Stein et al., 1994) is believed to have exerted a control on the aftershock triggering across a broad spectrum of spatial and temporal scales in the Longmen Shan range. It is worth mentioning that the buildings and other constructions were much seriously damaged on the hanging wall block than on the

Table 3 Orientations of coseismic ruptures and slickensides.

Latitude (°)	Longitude (°)	Fault plane Strike/Dip	Slickenside Pitch	
Yingxiu-Beic	huan fault			
31.0837	103.5645	252, 71		
31.0837	103.5645	250, 75		
31.1453	103.6918	223, 78	75 SW	
31.1453	103.6918	220, 80	78 SW	
31.1453	103.6918	225, 78	35 SW	
31.1453	103.6918	220, 75	45 SW	
31.1453	103.6918	245, 72	32 SW	
31.8322	104.4602	235, 80		
31.8322	104.4602	239, 68	50 SW	
31.8322	104.4602	245, 75	40 SW	
31.8326	104.4609	210, 80	30 SW	
Anxian-Guar	xian fault			
31.45	104.1626	246, 46		
31.3984	104.1182	240, 60		
31.4616	104.1655	250, 56		

footwall block across these coseismic ruptures (e.g., Yingxiu town and the Beichuan County town).

Fault-valve action

As mentioned before, the 12 May 2008 Wenchuan earthquake involved close-to-pure reverse slip on the principal listric faults dipping steeply (>60–80°, Table 2 and Figure 9) to the northwest in the 10–15 km thick uppermost crust. The sequential activation of the high-angle reverse faults in the Longmen Shan formed a characteristic margin between the Songpan-Ganzi terrane and the Sichuan Basin, which has the steepest topographic gradient of any edge of the modern plateaus. These rupture planes dip much steeply than the most favored dip angle (θ) for reverse-fault earthquakes (θ = 26.6 for most rocks with a frictional coefficient μ = 0.75). assuming horizontal maximum compressive stress (Anderson's model). The minimum ratio of the effective stresses (σ_1^*/σ_3^*), which is required to reactivate a reverse fault, is governed by the frictional failure criterion related to the so-called fault-valve behavior (Sibson et al., 1988):

$$(\sigma_1^*/\sigma_3^*) = (1 + \mu \operatorname{ctg}\theta) / (1 - \mu \operatorname{ctg}\theta)$$
 (1)

In this equation, $\sigma_1^* = \sigma_1 - P_f$, and $\sigma_3^* = \sigma_3 - P_f$, where σ_1 and σ_3 are the maximum and minimum principal stresses, respectively; and P_f is the pore-fluid pressure. The ratio of σ_1^*/σ_3^* has the minimum value ($\sigma_1^*/\sigma_3^* = 4$ or $\sigma_1 - \sigma_3 = 3$) when the reverse fault has an optimal dip angle of 26.6 because $\mu = 0.75$ for most rocks except those of serpentinite and mica-rich schists. In other words, any faults dip-

ping more than 45° are unfavorably oriented for reverse slip (earthquake) in the stress field. In order to activate or reactivate a reverse fault with $\theta > 53.2^{\circ}$ (the most likely case for the coseismic faults within the uppermost crust of the Longmen Shan range), σ_1^*/σ_3^* should be negative. The negative value of σ_1^*/σ_3^* implies that the fluid pressure P_f should be higher than σ_3 which is the lithostatic load in the compressional regime, that is, the rock-mass within the seismogenic zone is fluid-overpressured. Hence, the occurrence of an earthquake similar to the 12 May 2008 event should be relatively rare because it cannot be induced without some combination of considerably increasing fluid pressure and tectonic differential stress. The above analysis also provides a viable explanation for the relatively long average recurrence interval for earthquakes in the central and southern segments of the Longmen Shan range (e.g., the Dujiangyan and Wenchuan areas) which had been free from severe earthquakes for at least the last 2,500 years until 12 May 2008. The fact that the reverse or right-reverse oblique slip took place on steeply (50–80°) dipping fault planes, which are apparently unfavorably oriented for activation/reactivation, explains why the Wenchuan earthquake was so violent in terms of released energy because the faults were activated under extremely high levels of both regional tectonic stress and fluid overpressure, which had accumulated during the long interseismic period.

The degree of fluid overpressuring, which consequently affects the fault failure or frictional strength, varies with time. Fluid overpressuring triggers rock fractures and fault slip (earthquake), while dilatational fractures and frictional slip (the permeability of fault rocks is highest immediately post-failure) cause abrupt drops in fluid pressure (upward discharge of overpressurized fluids), resulting in mineral deposition in the fractured zone (e.g., forming calcite or quartz veins). The hydrothermal precipitation, seismic gouge compaction and crack sealing by pressure solution mass transfer (Gratier et al., 2003) consequently reduce the porosity and permeability of the fault zone, allowing reaccumulation of fluid overpressure and decreasing fault strength through the interseismic period before the next failure episode (Sibson, 1992). The processes described above are cycling: interseismic P_f increase, coseismic slip, and postseismic mineral deposition. For the first approximation, the recurrence interval for earthquakes for a given locality should correspond to the period of fluid-pressure fluctuation. An approximate estimation based on the fault-valve behavior suggests that the average recurrence interval for a M_s=8 earthquake should be in the general range of 3,000-12,000 years in the Longmen Shan region. Based on the coseismic slip of 3-9 m and the GPS velocity of ~1 mm/yr, one can easily obtain an average recurrence interval of 3,000-9,000 yr. An average recurrence interval of 2,000-10,000 yr was estimated by Burchfiel et al. (2008) based on the denudation rate of the Pengguan and Baoshan crystalline complexes. All these estimations are consistent within the uncertainty.

New interpretation of GPS data

GPS, a technique to measure the relative horizontal motion velocity between tectonic blocks, has been extensively applied to the Tibetan plateau and its surrounding regions (Chen et al., 2000; Zhang et al., 2004). The GPS velocities between the Indian and Eurasian plates vary from 28.0 mm/yr to 34 mm/yr, increasing gradually from central Himalaya to the eastern Himalayan Syntaxis (Zhang et al., 2004). Within the Tibetan plateau, the Lhasa and Qiangtang blocks west of 95° longitude move to N30°-47°E at the rate of 27-30 mm/yr (Figure 2). The eastern portion of the Qiangtang terrane, located south of the left-lateral Xianshuihe fault, moves southeast relative to the Sichuan Basin at a rate of 28 ±5 mm/yr. The Qaidam Basin and the Songpan-Ganzi terrane north of the Kunlun fault move to N60°E at rates of 12–14 mm/yr. However, the convergence across the Longmen Shan range is slow: <2 mm/yr across the Min Shan, ~1 mm/yr across the northeastern segment from Anxian to Qingchuan, and <1.5 mm/yr across the southwestern segment

from Luding to Baoxing and the central segment from Baoxin to Maoxian. Right-lateral slip of ~1 mm/yr occurs along the northeastern segment of the Longmen Shan. GPS data were misinterpreted as an evidence for inactivity of the Longmen Shan faults and thus impossibility of strong earthquakes in the region (Chen et al., 2000; Zhang et al., 2002, 2004; Deng et al., 2006). These authors claimed that little movements take place along the Longmen Shan faults due to the huge amount of crustal material south of the Xianshuihe-Anninghe-Xianjiang sinistral strike-slip fault zone moving southeast from southeastern Tibet and northwestern Yunnan to southeastern Yunnan, and to an important clockwise rotation around the eastern Himalayan Syntaxis (Zhang et al., 2004).

It is important to note that 4 earthquakes with M_s 8.0 and 10 events with M_s =7.0–7.9 were located in the regions where the GPS velocities are markedly low or where the horizontal motion radically changes direction. The low GPS velocities are found systematically at the fronts of the enlarging Tibetan plateau against rheologically strong blocks such as the Sichuan Basin, Ala Shan and Ordos blocks. It is very likely that these front zones are characterized by the development of steep-to-vertical close-to-pure reverse or reverse oblique slip faults across which the GPS technique hardly detects the horizontal convergence rates during an interseismic period. In the fault zones against rheologically strong blocks, differential stress can accumulate to such a high level that the Ms≥7.0 earthquake rupturing can result.

Conclusions

- (1) The 12 May 2008 Wenchuan earthquake (M_s=8.0) occurred within the context of long-term uplift of the Longmen Shan range as a result of the eastward extrusion of the crustal materials from the Tibetan plateau against the rheologically strong crust of the Sichuan Basin. The range is characterized by a Pre-Sinian crystalline complex constrained by the Maoxian-Wenchuan-Kangding ductile detachment at the western margin and the Yingxiu-Beichuan-Luding ductile thrust at the eastern margin. The uplift of Longmen Shan was initiated by the intracontinental subduction between the Songpan-Ganzi terrane and the Yangtze block during the Pre-Cenozoic. The uplift rate was increased considerably by the collision between the Indian and Eurasian plates since ~50 Ma.
- (2) The Wenchuan earthquake started on the northwest-dipping fault (238, 59), known as the Yingxiu-Beichuan-Qingchuan fault and propagated unilaterally to the northeast over a distance of ~275 km. The maximal vertical and horizontal components of the co-seismic slip are 8.0 m and 10.0 m, respectively. From SW to NE along the fault, the thrust component decreases gradually while the dextral strike-slip component increases. The tremor moved east to the Guanxian-Anxian fault, forming a coseismic surface rupture of ~100 km long. This suggests that the M_S=8.0 earthquake from the Yingxiu-Beichuan-Qingchuan fault triggered the earthquakes on the Guanxian-Anxian fault.
- (3) The Wenchuan earthquake involved close-to-pure reverse or right-reverse oblique slip on steeply dipping fault planes which were unfavorably oriented for activation/reactivation and approached frictional lock-up in the regional horizontal compressional regime. The occurrence of coseismic slip on the steeply dipping faults implies some combination of extremely high levels of both regional tectonic and fluid overpressure.
- (4) In northeastern Tibetan plateau and its surrounding regions, large earthquakes with M_s≥7.0 occurred in the fault zones across which the GPS velocities are markedly low (<3 mm/yr). The low GPS velocity zones are indeed the fronts of the enlarging Tibetan plateau against the rheologically strong blocks (i.e., the Sichuan Basin, Ala Shan and Ordos blocks). The faults are steeply dipping close-to-pure reverse faults, allowing tectonic stress and fluid pressure to accumulate to a critically high level for large earthquake nucleation and propagation.

Acknowledgments

This project was supported by the China Geological Survey and the NSERC of Canada. Qian Wang and Shengsi Sun are thanked for discussion; Miao Zhang, Cuiping Xu and Yveric Rousseau for drawing the figures; and Prof. Jacques Martignole for constructive review of the manuscripts.

References

- Burchfiel, B.C., Royden, L.H., van der Hilst, R.D., Hager, B.H., Chen, Z., King, R.W., Li, C., Lu, J., Yao, H., and Kirby, E., 2008, A geological and geophysical context for the Wenchuan earthquake of 12 May 2008, Sichuan, China: GSA Today, v.18, no. 7, doi: 10.1130/GSATG18A.1.
- Chen, S.F. and Wilson, C.J.L., 1995, Emplacement of the Longmen Shan thrust-nappe belt along the eastern margin of the Tibetan Plateau: Journal of Structural Geology, v. 18, pp. 413–430.
- of Structural Geology, v. 18, pp. 413–430.

 Chen, Z.L., Burchfiel, B.C., Liu, Y., King, R.W., Royden, L.H., Tang, W., Wang, E., Zhao, J., and Zhang, X., 2000, Global positioning system measurements from eastern Tibet and their implications for India/Eurasia intercontinental deformation: Journal of Geophysical Research, v. 105, pp. 16215–16227.
- Clark, M.K. and Royden, L.H., 2000, Topographic ooze: Building the eastern margin of Tibet by lower crustal flow: Geology, v. 28, pp. 703–706.
- Deng, Q.D., Ran, Y.K., Yang, X.P., Min, W., and Chu, Q.Z., 2007, Map of Active Tectonics in China: Seismological Press, Beijing.
- Gratier, J.P., Favreau, P., and Renard, F., 2003, Modeling fluid transfer along California faults when integrating pressure solution crack sealing and compaction processes: J. Geophys. Res., 108, B2, 2104, doi:10.1029/ 2001JB000380.
- Jia, D., Chen, Z.X., Jia, C.Z., Wei, G.Q., et al., 2003, Structural features of the Longmen Shan fold and thrust belt and development of the western Sichuan foreland basin, Central China: Geological Journal of Chian Universities, v. 9, pp.402–410.
- Parsons T, Ji C, and Kirby E., 2008, Stress changes from the 2008 Wenchuan earthquake and increased hazards in the Sichuan basin. Nature, 454: 509–510.
- Royden, L.H., Burchfiel, B.C., King, R.W., et al., 1997, Surface deformation and low crustal flow in eastern Tibet: Science, v. 276, pp. 788–790.
- Sibson, R.H., 1992. Implications of fault-valve behavior for rupture nucleation and recurrence: Tectonophysics 211, 283–293.
- Sibson, R.H., Robert, F., and Poulsen, H., 1988, High-angle reverse faults, fluid-pressure cycling, and mesothermal gold-quartz deposits: Geology 16, 551–555.
- Song, W.H., 1989, On nappe structure at northern sector of Longmen mountains and its oil and gas prospects: Actual Gas Industry, v. 9, pp. 2–9.
- Stein R.S., King, G.C.P., and Lin, J., 1994, Stress triggering of the 1994 M=6.7 Northridge, California, Earthquake by its predecessors. Science, 265, 1432–1435.
- Wallis, S., Tsujimori, T., Aoya, M., et al., 2003, Cenozoic and Mesozoic metamorphism in the Longmen Shan orogen: implications for geodynamic models of eastern Tibet: Geology, v.31, pp. 745–748.
- Wang, E.Q., Meng, Q.R., and Chen Z.L., 2001, Early Mesozoic left-lateral movement along the Longmen Shan fault belt and its tectonic implications, Earth Science Frontiers, v. 8, pp. 375–384.
- Wittinger, G., Tapponnier, P., Poupinet, G., et al., 1998, Tomographic evidence for localized lithospheric shear along the Altyn Tagh fault: Science, v. 282, pp. 74–76.
- Xu, Z.Q., Hou, L.W., Wang, Z.X., et al., 1992, Orogenic processes of the Songpan-Garzi orogenic belt of China: Geological Publishing House, Beijing, pp. 1–190.
- Xu, Z.Q., Jiang, M., and Yang, J.S., 1999, Mantle diaper inward intracontinental subduction: A discuss on the mechanism of uplift of the Qinghai-Tibet plateau: Geological Society of America, Special Paper, v. 328, pp. 19–31.
- Xu, Z.Q., Li, H.Q., Hou, L.W., Fu, X.F., Chen, W., Zeng, L.S., Cai, Z.H., and Chen, F.Y., 2007, Uplift of the Longmen-Jinping orogenic belt along the eastern margin of the Qinghai-Tibet Plateau: Large-scale detachment faulting and extrusion mechanism: Geological Bulletin of China, v.26, pp. 1262–1276.

- Zhang, P.Z., Shen, Z., Wang, M., Gan, W., Burgmann R., Molnar, P., Wang, Q., Niu, Z., Sun, J., Wu, J., Sun, H., and You, X., 2004, Continuous deformation of the Tibetan Plateau from Global Positioning System data: Geology, v.32, pp. 809–812.
- Zhang, P.Z., Wang, Q., and Ma, Z.J., 2002, GPS velocity field and active crustal deformation in and around the Qinghai-Tibet Plateau: Earth Science Frontiers, v.9, pp. 442–450.

Zhiqin Xu is Research Professor at Institute of Geology, Chinese Academy of Geological Sciences, and member of Chinese Academy of Sciences. She obtained her PhD from University of Montpellier, France in 1986. Her current research interests cover the deformation process and mechanism for rocks from various levels of continental lithosphere and tectonics of major orogenic belts. She has been playing a leading role in Chinese Continental Scientific Drilling (CCSD) project on the Sulu high- to ultrahigh- pressure (HP/ UHP) metamorphic belt and, for more than ten years, in the Sino-French collaboration projects for studying the Tibetan plateau and its marginal orogenic belts.



Shaocheng Ji is professor of Earth Sciences in the Department of Civil, Geological and Mining Engineering, Ecole Polytechnique de Montreal (Canada), obtained his B.Sc. from Nanjing University (China), and Ph.D. from the UniversitŽ de Montpellier II (France). He has been involved in research and teaching in petrophysics, structural geology and geophysics for over 20 years. He is author of 3 books and over 80 research papers.



Haibing Li is Research Professor at the Institute of Geology, Chinese Academy of Geological Sciences, and is Director of the Continental Dynamics Laboratory under the Institute. He obtained his Ph.D. in 2000 from the CAGS. His scientific interests are focused on tectonic geomorphology and active tectonics, mountain building and neotectonic structures.

